

MONTHLY 43 GHz VLBA POLARIMETRIC MONITORING OF 3C 120 OVER 16 EPOCHS: EVIDENCE FOR TRAILING SHOCKS IN A RELATIVISTIC JET

JOSÉ-LUIS GÓMEZ,¹ ALAN P. MARSCHER,² ANTONIO ALBERDI,¹ SVETLANA G. JORSTAD,² AND IVÁN AGUDO¹

Received 2001 August 25; accepted 2001 October 3; published 2001 October 31

ABSTRACT

We present a 16 month sequence of monthly polarimetric 43 GHz VLBA images of the radio galaxy 3C 120. The images probe the inner regions of the radio jet of this relatively nearby superluminal radio galaxy at a linear resolution of $0.07 h_{65}^{-1}$ pc ($H_0 = 65 h_{65} \text{ km s}^{-1} \text{ Mpc}^{-1}$). We follow the motion of a number of features with apparent velocities between 4.01 ± 0.08 and $5.82 \pm 0.13 h_{65}^{-1} c$. A new superluminal knot, moving at $4.29 \pm 0.16 h_{65}^{-1} c$, is observed to be ejected from the core at a time coincident with the largest flare ever observed for this source at millimeter wavelengths. Changes in the position angle of this component, as well as a progressive rotation of its magnetic polarization vector, suggest the presence of a twisted (resembling a helix in projection) configuration of the underlying jet magnetic field and jet geometry. We identify several knots that appear in the wake of the new superluminal component, moving at proper motions ~ 4 times slower than any of the other moving knots observed in 3C 120. These features have properties similar to those of the “trailing” shocks seen in relativistic, time-dependent, hydrodynamical, and emission simulations of compact jets. Such trailing compressions are triggered by pinch-mode jet-body instabilities caused by the propagation of a strong perturbation, which we associate with the new strong superluminal component.

Subject headings: galaxies: active — galaxies: individual (3C 120) — galaxies: jets — polarization — radio continuum: galaxies

1. INTRODUCTION

The radio galaxy 3C 120 (redshift $z = 0.033$) is a powerful and variable emitter of radiation at radio to X-ray frequencies, probably powered by a central black hole of at least $3 \times 10^7 M_\odot$ (Maraschi et al. 1991; Wandel, Peterson, & Malkan 1999). It was among the first radio jets in which apparent superluminal motion was detected (Seielstad et al. 1979; Walker, Benson, & Unwin 1987; Benson et al. 1988; Walker 1997). Previous observations using the Very Long Baseline Array (VLBA) at 22 and 43 GHz (Gómez et al. 1998) reveal a very rich inner jet structure containing up to 10 different superluminal components. Coordinated Millimeter VLBI Array observations at 86 GHz (Gómez, Marscher, & Alberdi 1999), at an angular resolution of $54 \mu\text{as}$, provide an upper limit to the size of the core of ~ 1 lt-month. Results from long-term milliarcsecond-scale monitoring at 1.7, 5, and 10.7 GHz allowed Walker et al. (2001) to determine superluminal motions up to at least 150 pc in projection from the core as well as to find evidence for stationary features suggestive of a helical pattern viewed in projection.

With further monitoring at a higher frequency, consisting of 16 monthly polarimetric 22 GHz VLBA observations of 3C 120, Gómez et al. (2000) explored a more compact region in the jet, where superluminal components undergo variations in total and linearly polarized flux densities on timescales of months.³ In this Letter, we present 43 GHz images corresponding to the same epochs as the 22 GHz observations presented in Gómez et al. (2000).

2. OBSERVATIONS AND DATA ANALYSIS

We observed 3C 120 with the 10 antennas of the VLBA at a frequency of 43 GHz at the following epochs: 1997 November 10, 1997 December 11, 1998 January 11, 1998 February 7, 1998 March 9, 1998 April 10, 1998 May 9, 1998 June 11, 1998 July 11, 1998 August 13, 1998 September 16, 1998 October 26, 1998 December 3, 1999 January 10, 1999 February 10, and 1999 March 19. The data were recorded in a 1 bit-sampling VLBA format with 32 MHz bandwidth per circular polarization. Reduction of the data was performed with the AIPS software in the usual manner (e.g., Leppänen, Zensus, & Diamond 1995). Opacity corrections were introduced by solving for receiver temperature and zenith opacity at each antenna. The instrumental polarization was determined using the feed-solution algorithm developed by Leppänen et al. (1995). The feed D -terms (instrumental polarization) were found to be very consistent over all sources observed and to remain stable. The absolute phase offset between right- and left-circularly polarized data (which determines the polarization position angle calibration) was obtained by the comparison of the integrated polarization of the VLBA images of several compact sources (0420–014, OJ 287, BL Lac, and 3C 454.3) with 14 Very Large Array (VLA) observations at epochs 1997 November 21, 1997 December 14, 1998 January 15, 1998 February 12, 1998 March 7, 1998 April 8, 1998 June 9, 1998 July 11, 1998 August 14, 1998 September 19, 1998 October 29, 1998 November 28, 1999 February 17, and 1999 March 17. Estimated errors in the orientation of the polarization vectors vary from epoch to epoch but usually lie in the range of 7° – 15° , confirmed by the stability of the D -terms across epochs (J.-L. Gómez et al. 2001, in preparation).

3. RESULTS

The images, plotted in Figure 1, reveal a rich, variable structure in both total and linearly polarized intensity. In Figure 1, the epochs of observation are indicated to the right of each

¹ Instituto de Astrofísica de Andalucía, CSIC, Apartado 3004, 18080 Granada, Spain; jlgomez@iaa.es, antxon@iaa.es, ivan@iaa.es.

² Institute for Astrophysical Research, Boston University, 725 Commonwealth Avenue, Boston, MA 02215; marscher@bu.edu, jorstad@rjet.bu.edu.

³ A movie generated from these 16 total and polarized intensity images can be downloaded at Science On-line (<http://www.sciencemag.org/feature/data/1052657.shl>).

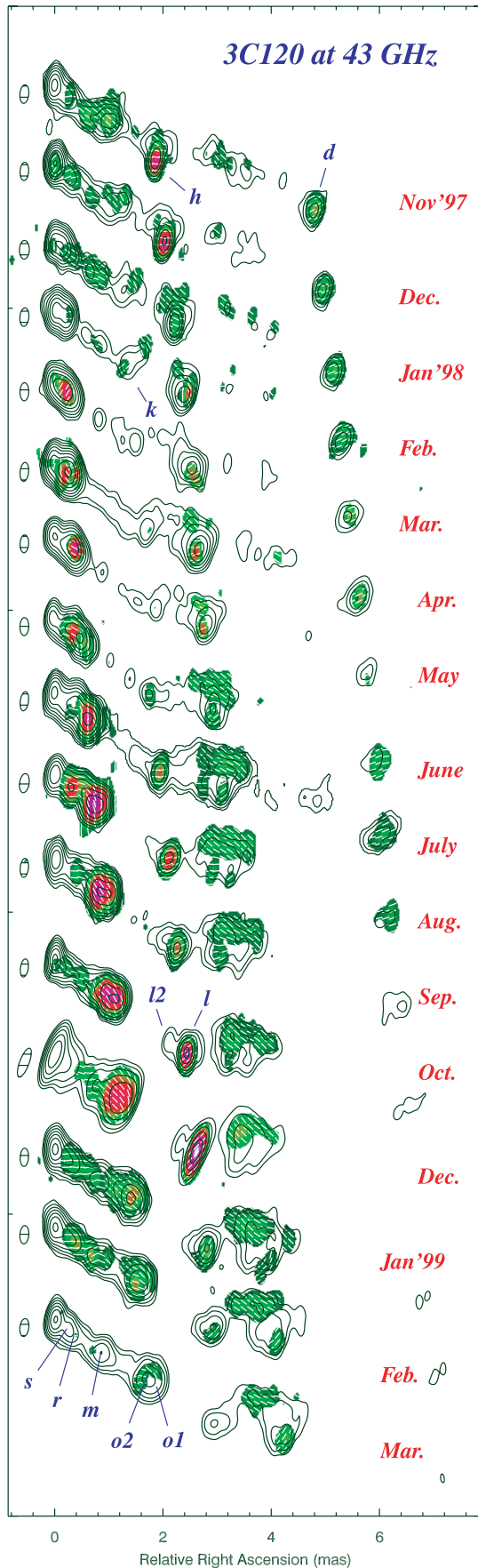


FIG. 1.—VLBA images of 3C 120 at 43 GHz. See text.

image. The vertical image separation is proportional to the time difference between epochs of observation. Contours give the total intensity, colors (on a linear scale from green to white) show the polarized intensity, and bars (of unit length) indicate the direction of the magnetic polarization vector. Synthesized beams are plotted to the left of each image, with a typical size of 0.35×0.16 mas. The peak brightness (rms noise) in polarization corresponds to $32.4 \text{ mJy beam}^{-1}$ ($1.4 \text{ mJy beam}^{-1}$). Contour levels for all epochs are in factors of 2 of the bottom level of $4.4 \text{ mJy beam}^{-1}$, except for epochs 1998 February, 1998 May, 1998 July, 1998 August, 1998 October, 1998 December, and 1999 January for which the bottom contour level is $8.8 \text{ mJy beam}^{-1}$. For epoch 1998 June, an extra contour at $2.2 \text{ mJy beam}^{-1}$ has been plotted. No data were obtained in MK station for epoch 1998 December, which resulted in a larger synthesized beam.

In order to identify and follow discrete features across epochs, we performed model fits of the u - v data with circular Gaussian components using the software Difmap (Shepherd 1997), which was also used to edit the data and make the final images. Figure 2 shows the positions and magnetic polarization direction for the fitted components at all epochs. Inspection of this figure reveals that at a distance of approximately 2 mas from the core (the closest distance at which we can resolve the jet across its width), bright features usually lie near the edge of the jet, suggesting limb brightening. This stratification is even more apparent in polarization: magnetic vectors on the northern side of the jet are oblique to the jet axis but constant in orientation, while those on the southern side rotate as the polarized emission features move downstream (e.g., components h and l in Fig. 2). This is similar to the behavior observed at 22 GHz (Gómez et al. 2000).

3.1. Superluminal Components

Because of the complexity and temporal variability of the jet, some of the fitted components cannot easily be identified across epochs. We concentrate our discussion on those features that can be followed reliably. Six of these components, those labeled in Figure 1 as o (containing components o1 and o2), l2, l, k, h, and d, separate from the core at apparent superluminal velocities (proper motions) of 4.29 ± 0.16 (1.83 ± 0.07), 5.38 ± 0.08 (2.29 ± 0.04), 5.10 ± 0.14 (2.17 ± 0.06), 5.82 ± 0.13 (2.48 ± 0.05), 4.12 ± 0.06 (1.75 ± 0.03), and 4.01 ± 0.08 $h_{65}^{-1} c$ ($1.71 \pm 0.03 \text{ mas yr}^{-1}$), respectively. The separation of these components from the core versus time is plotted in Figure 3.

As observed at 22 GHz (Gómez et al. 2000), components h and l brighten markedly when reaching a distance of about 3 mas from the core (see Figs. 1 and 2). Gómez et al. explained this brightening, accompanied by a rotation of the magnetic polarization vector, as an interaction between the jet and a cloud with properties intermediate between those of the broad and narrow emission-line regions.

The inner jet structure in Figure 1 is dominated by the appearance of a new component near the beginning of the largest millimeter-wave flare ever observed in 3C 120 (H. Teräsranta 2001, private communication). By epoch 1997 December 14, the core had brightened significantly (see Fig. 4), after which the new component (o), appeared downstream of the core (Fig. 1). Figure 4 shows that component o presents an extended emission structure that can be split into three different features (those marked in red in Fig. 4) between 1998 January 11 and April 10. These probably do not represent distinct entities but rather correspond to the complexity in the internal brightness

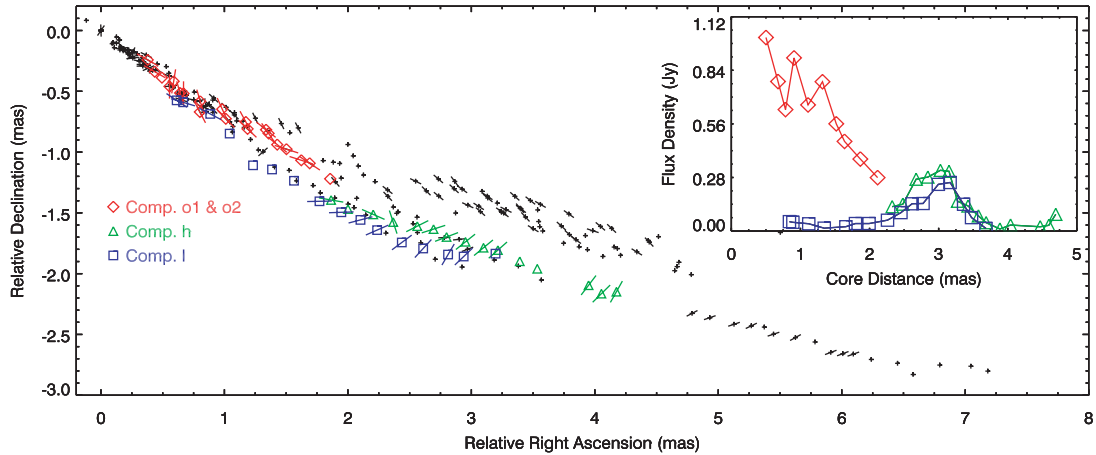


FIG. 2.—Positions and magnetic polarization vector orientations of the components obtained from model fitting of the images shown in Fig. 1. Components o1, o2, h, and l have been highlighted with different symbols and colors, with their light curves plotted in the inset panel. The integrated flux density is plotted at the position of the brightness centroid for components o1 and o2.

distribution, reminiscent of the pattern of major disturbances in numerical simulations (Gómez et al. 1997). By epoch 1998 May 9, the front of knot o is further resolved into two subcomponents, labeled o1 and o2, with proper motions of $1.87 \pm 0.05 \text{ mas yr}^{-1}$ ($4.40 \pm 0.12 h_{65}^{-1} c$) and $1.78 \pm 0.05 \text{ mas yr}^{-1}$ ($4.19 \pm 0.11 h_{65}^{-1} c$), respectively. The epoch of ejection (i.e., the extrapolated date of coincidence with the core) of component o1 is 1998.07 ± 0.03 (see Fig. 4).

Although components o1 and o2 move with a relatively constant proper motion, Figure 5a (see also Fig. 2) shows that the lines between their positions and that of the core vary by 7° as they move between ~ 0.5 and 2.0 mas from the core. Furthermore, these variations in position angle are accompanied by the rotation of the magnetic polarization vectors with respect to the local jet axis, as shown in Figure 5b (see also Fig. 2). The initially perpendicular magnetic vector at epoch 1998 March 9 is observed to align with the jet axis by 1998 May 8. This is followed by a rotation of about 60° by 1998 June 11. The magnetic vector subsequently rotates more slowly in components o1 and o2 until it becomes approximately aligned to the jet axis during the final epochs. Opacity effects, which can produce a rotation of 90° (as observed in OJ 287; Gabuzda & Gómez 2001), could only be present at epoch 1998 March 9, when component o has a nearly flat spectrum ($\alpha \sim -0.06$, $S_\nu \propto \nu^\alpha$); at the other epochs, components o1 and o2 have steep, optically thin spectra.

Although Faraday rotation could contribute to the observed

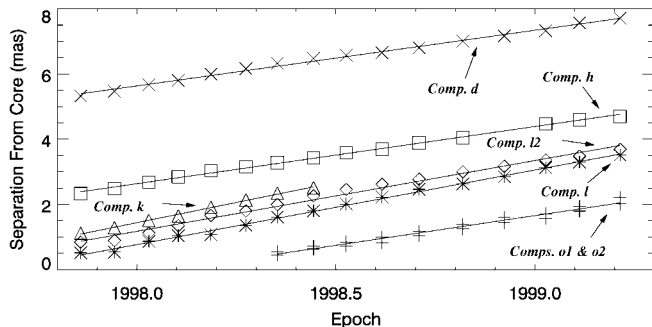


FIG. 3.—Projected angular distance from the core as a function of time for the superluminal components found in 3C 120. The lines show a minimum χ^2 linear fit for each component. A common fit has been used for components o1 and o2.

rotation of the magnetic polarization vectors, an alternative interpretation would be the existence of an underlying helical magnetic field with a pitch angle that would progressively increase until the magnetic field becomes aligned (as observed at larger scales; Walker et al. 1987). This would be in agreement with the observed variation in the position angles of the core-component separations and the twisted internal structure of component o, the latter of which is most clearly visible at epochs 1998 June 11, July 11, and August 13 (see Fig. 1). This interpretation would also agree with the suggested helical pattern at larger scales (Walker et al. 2001).

3.2. Trailing Components

By epoch 1998 May 9, we can distinguish two emission regions in the newly ejected component o: the front section (subcomponents o1 and o2, plotted in green in Fig. 4) and the back section (p, plotted in blue in Fig. 4). The subsequent evolution of these two emission regions is significantly differ-

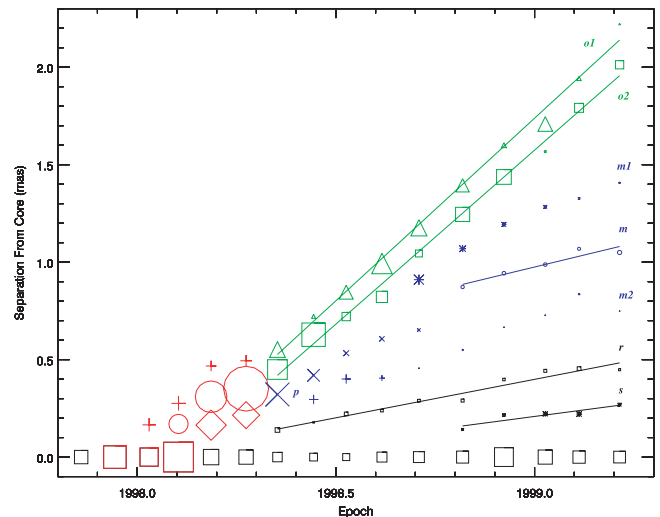


FIG. 4.—Projected angular distance from the core vs. time for the jet features between component o1 and the core. The symbol size is proportional to the component's total flux density. Those features associated with the initial evolution of component o are plotted in red. By epoch 1998 May 9, this component can be resolved into two different sets of subcomponents, each with a different development: those marked in green (for components o1 and o2) and those in blue, corresponding to the trailing components.

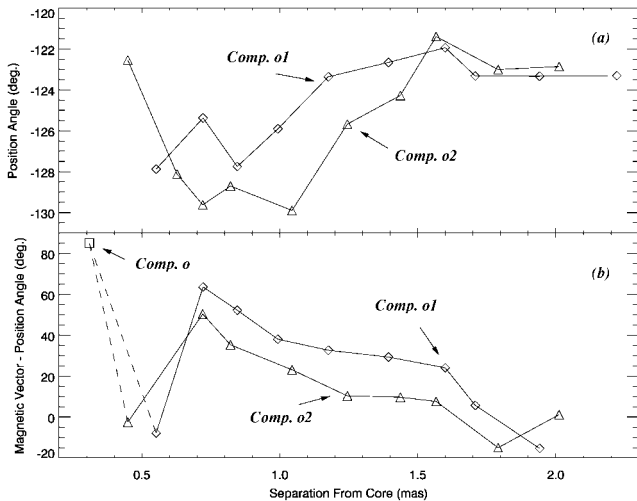


FIG. 5.—(a) Position angle and (b) orientation of the magnetic polarization vector relative to the core position angle for components o, o1, and o2 as a function of projected angular distance from the core.

ent: While subcomponents o1 and o2 move with a relatively constant proper motion, Figure 4 shows that component p splits into two parts that progressively decelerate and decrease in total flux more rapidly than do subcomponents o1 and o2. Acceleration is also observed to take place later in component m2. By epoch 1998 September 16, a similar split takes place, leading to the appearance of components m and m1. The evolution of the jet following the disturbance that created component o therefore involves steady, fast superluminal motion at the front, followed by the (in some cases temporary) appearance of slower secondary features in the wake.

The last epochs in Figures 1 and 4 show that the strongest feature in the wake of component o is that labeled m. This component, which maintains a relatively constant flux density of ~ 100 mJy, moves at an apparent speed of $1.16 \pm 0.22 h_{65}^{-1} c$ (0.49 ± 0.09 mas yr $^{-1}$). This is a factor of ~ 4 slower than any of the other moving components detected in 3C 120 (see Fig. 3). Images at 22 GHz (Gómez et al. 2000) also contain component m, but with a proper motion compatible with stationarity (-0.35 ± 1.10 mas yr $^{-1}$); however, the resolution was about twice as coarse as that at 43 GHz. The polarization of m is strong at 22 GHz, with a magnetic vector direction (relative to the direction between m and the core) of 24° , 19° , and 27° and a degree of polarization of 25%, 20%, and 15% at epochs 1999 January 10, 1999 February 10, and 1999 March 19, re-

spectively. Two components even closer to the core, labeled r and s, are also apparent in Figure 4. Their proper motions are the slowest detected in 3C 120: 0.40 ± 0.03 mas yr $^{-1}$ ($0.93 \pm 0.07 h_{65}^{-1} c$) and 0.27 ± 0.07 mas yr $^{-1}$ ($0.63 \pm 0.17 h_{65}^{-1} c$) for r and s, respectively.

The nature of the components that appear in the wake of component o is consistent with the characteristics of the trailing features that appear behind a major flow disturbance in relativistic time-dependent hydrodynamical and emission simulations of jets (Agudo et al. 2001). These simulations show that strong jet perturbations (which we associate with bright superluminal knots) interact with the underlying jet and external medium as they propagate. This leads to the formation of recollimation shocks and rarefactions in the wake of the main perturbation. These formations are triggered by pinch-body jet instabilities. Agudo et al. (2001) predict that trailing components should appear to split from the primary component rather than emerge from the core and to have significantly slower proper motions than that of the leading strong knot. The apparent velocities of the trailing features should range from subluminal closest to the core to more superluminal near the leading knot. This is in good agreement with the nature of component m, which indeed appears to split from component o and to move at a slower speed. Alternatively, component m may correspond to a reverse shock of component o that is slower than the forward shock represented by subcomponents o1 and o2 in this interpretation. The subluminal motions of components r and s are also consistent with the predictions for trailing components.

The good agreement between the changing emission pattern observed in 3C 120 and the structures predicted by two-dimensional, relativistic, cylindrically symmetric hydrodynamical and emission simulations (Agudo et al. 2001) points to the value of such computations for interpreting observations of real jets. Three-dimensional simulations that are now becoming available promise to provide even more realistic comparisons.

This research was supported in part by Spain's Dirección General de Investigación Científica y Técnica (DGICYT) grant PB97-1164, by US National Science Foundation (NSF) grant AST 98-02941, and by a Fulbright commission for the collaboration between Spain and the US. The VLBA and VLA are instruments of the National Radio Astronomy Observatory, a facility of the NSF operated under cooperative agreement by Associated Universities, Inc. We are grateful to Barry Clark for scheduling ad hoc VLA time in order to determine the polarization position angle calibration.

REFERENCES

- Agudo, I., Gómez, J.-L., Martí, J.-M., Ibáñez, J. M., Marscher, A. P., Alberdi, A., Aloy, M.-A., Hardee, P. E. 2001, *ApJ*, 549, L183
 Benson, J. M., Walker, R. C., Unwin, S. C., Muxlow, T. W. B., Wilkinson, P. N., Booth, R. S., Pilbratt, G., & Simon, R. S. 1988, *ApJ*, 334, 560
 Gabuzda, D. C., & Gómez, J. L. 2001, *MNRAS*, 320, L49
 Gómez, J.-L., Marscher, A. P., & Alberdi, A. 1999, *ApJ*, 521, L29
 Gómez, J.-L., Marscher, A. P., Alberdi, A., Jorstad, S. G., & García-Miró, C. 2000, *Science*, 289, 2317
 Gómez, J.-L., Marscher, A. P., Alberdi, A., Martí, J.-M., & Ibáñez, J.-M. 1998, *ApJ*, 499, 221
 Gómez, J.-L., Martí, J.-M., Marscher, A. P., Ibáñez, J.-M., & Alberdi, A. 1997, *ApJ*, 482, L33
 Leppänen, K. J., Zensus, J. A., & Diamond, P. J. 1995, *AJ*, 110, 2479
 Maraschi, L., Chiapetti, L., Falomo, R., Garilli, B., Malkan, M., Tagliaferri, G., Tanzi, E. G., & Treves, A. 1991, *ApJ*, 368, 138
 Seielstad, G. A., Cohen, M. H., Linfield, R. P., Moffet, A. T., Romney, J. D., Schilizzi, R. T., & Shaffer, D. B. 1979, *ApJ*, 229, 53
 Shepherd, M. C. 1997, in *ASP Conf. Ser. 125, Astronomical Data Analysis Software and Systems VI*, ed. G. Hunt & H. E. Payne (San Francisco: ASP), 77
 Walker, R. C. 1997, *ApJ*, 488, 675
 Walker, R. C., Benson, J. M., & Unwin, S. C. 1987, *ApJ*, 316, 546
 Walker, R. C., Benson, J. M., Unwin, S. C., Lystrup, M. B., Hunter, T. R., Pilbratt, G., & Hardee, P. E. 2001, *ApJ*, 556, 756
 Wandel, A., Peterson, B. M., & Malkan, M. A. 1999, *ApJ*, 526, 579